Numerical Simulation of Erosion on Aluminium Plate with a Cylindrical Hole

Halima Hadžiahmetović[1], Ejub Džaferović[1], Sanda Midžić Kurtagić[1], Rejhana Blažević[1*]

[1] Faculty of Mechanical Engineering, University of Sarajevo, Vilsonovo šetalište 9, Sarajevo, Bosnia and Herzegovina

* Corresponding author's e-mail: muhamedagic@mef.unsa.ba

ABSTRACT

The purpose of the present study is to simulate erosion on the aluminium plate with a cylindrical hole caused by solid particles after passing through 90° elbow, using the Computational Fluid Dynamics (CFD), the Discrete Phase Model (DPM), and erosion equations. Discrete trajectories of solid particles are calculated using the Lagrangian approach, while the simulation of the fluid was obtained by solving the fluid motion equation using the Eulerian approach. Supplementary sub-models are incorporated into the software to enhance the accuracy of particle trajectory calculations within the simulated geometry. These sub-models include collisions of solid particles with walls (stochastic model) and erosion model. The numerical simulation results obtained in this paper were compared with the existing experimental results from the group of authors, demonstrating a good match. The paper provides the main characteristics of the mathematical model, along with the interpretation of results and a discussion, with the key findings highlighted in the conclusion. The findings indicate that erosion process is significantly influenced by both the particle impact velocity and impact angle, which are key parameters in many erosion equations. Furthermore, it is observed that the velocity of the particles is consistently lower than the mean velocity of the air. Additionally, the angle at which the particles impact the aluminium plate is not always exactly 90° due to multiple collisions with the wall, signifying that the particles do not move exclusively vertically.

Keywords: pneumatic conveying, solid particle, continuous phase, discrete phase, erosion model.

INTRODUCTION

Erosion, which occurs as a result of the abrasive materials acting on various components of the system, represents a serious issue and significant challenge, in pneumatic conveying systems. The occurrence of erosion in pneumatic conveying system elements is heavily influenced by the characteristics of transported materials and solid surfaces, including factors such as particle impact velocity, particle impact angle, particle properties and the hardness of the target material [1-3]. The fundamental cause of erosion is the interaction between particles and wall, resulting in the removal of wall materials. Erosive wear depends on both, the impact angle of particles on the material's surface and the velocity of solid particles, constituting two key parameters that dictate the

erosion of the target material. The impact angle varies between 0º and 90º and depends on both fluid-particle and particle-particle interactions. Accurate prediction of erosion is essential for identifying locations prone to severe erosion [4-6]. Numerous models for solid particle erosion have been proposed to estimate erosion rates for various components [2-4]. Several studies have explored numerical models to predict particle-induced erosion [4, 6, 7]. Typically, researchers employ the standard Reynolds-averaged Navier–Stokes (RANS) equations to predict fluid flow through elbows using the Eulerian approach, followed by Lagrangian approach for tracking of particles [1, 2, 6]. Meng and Ludema [8] compiled 28 erosion prediction equations that were specifically developed for solid particle–wall erosion and outlined the 33 parameters employed in these

models. Lain et al. [9] analyzed various transport effects on spherical solid particle erosion in a pipe bend of a pneumatic conveying system. The erosion model they applied was validated using experimental data, showing satisfactory agreement. They demonstrated that factors such as wall surface structure, especially wall roughness incorporated in the collision model, and assumptions about the wall friction coefficient significantly influence erosion predictions. Zhou [10] investigated the effect of particle shape, considering non-spherical particles in their modelling. Nguyen et al. [11] conducted an experimental study to demonstrate the effect of particle size on the erosion rate. Finnie [12] demonstrated that the erosion rate is proportional to the square of the particle velocity. Li et al. [13] simulated the continuous bend erosion process in various directions using the dense discrete particle model. They conducted numerical simulations on seven continuous elbows with different orientations, considering straight pipe lengths and particle sizes as variables. The findings revealed that dense discrete particle model demonstrated high accuracy in predicting the distribution of continuous bend erosion processes in different directions. Hong et al. [14] investigated the effects of gas flow rate, solid mass flow rate, particle diameter, and other factors on the maximum erosion rate. The study revealed a negative correlation between the maximum erosion rate and both pipe diameter and elbow curvature radius. Hadziahmetovic et al. [15] conducted simulations on the pneumatic conveying of particles in a 90° bend, comparing the results with the existing measurements from group of authors [16]. The numerical simulation showed a satisfactory agreement with the measurements, particularly in the region of the highest erosion. Additionally, Pereira et al. [17] explored numerical models to predict erosion caused by particles in a 90-degree curved elbow pipe. Four different erosion rate correlations, namely Ahlert, Neilson and Gilchrist, Oka, and Zhang models, were tested. Experimental data was utilized to assess the accuracy of numerical predictions for the erosion rate. The impact of numerical parameters, such as the number of computational particles, as well as the models for coefficients of restitution, friction, and surface roughness, was examined. The results demonstrated that the Oka model is the most suitable for predicting erosion in this particular case, as it provided the best agreement with the experimental penetration ratio in terms of both magnitude and position.

The primary objective of this paper is to predict erosion on an aluminium plate with a cylindrical hole caused by solid particles after passing through an elbow. The fluid–solid flow was addressed using the Eulerian–Lagrangian approach. Various parameters, including the mean erosion rate, mean angle of particle impact on the elbow wall, erosion depth, particle velocity, and particle concentration on the opening surface, were computed. Basic information on the experimental setup, as conducted by a group of authors in [18], is provided in this paper. Additionally, the steps employed to enhance our simulation results are listed and clarified. A comparison between the numerical simulation results presented in this paper and the experimental outcomes from the aforementioned research group demonstrates a significant level of agreement.

MATERIAL AND METHODS

In this study, the Euler–Lagrange approach is utilized. The erosion model is described using Finnie's proposed mechanism. The following sections provide details on the modelling of both phases, along with the particle-wall rebound model and Finnie erosion model.

Continuous phase

The simulation of the fluid (air) was conducted by solving the fluid motion equation (Navier-Stokes equations) using the Eulerian approach. To simulate the continuous phase, the so-called "RSM" (Reynolds Stress Model) was used, which belongs to the group of "Reynolds-Averaged Navier-Stokes" (RANS) models. Air flow can be described by transport equations based on the principles of conservation of mass and conservation of momentum [19, 20].

$$\frac{\partial \rho}{\partial t} + \nabla \cdot (\rho u) = 0 \qquad (1)$$

$$\frac{\partial}{\partial t}(\rho u) + \nabla \cdot (\rho uu) = \underbrace{-\nabla p}_{\substack{\text{Pressure} \\ \text{forces}}} + \underbrace{\nabla \cdot \left(\eta (\nabla u + \rho \overline{u'}\,\overline{u'}) \right)}_{\substack{\text{Viscous} \\ \text{forces}}} \qquad (2)$$

where: ρ – fluid density, u – fluid velocity, ∇ – gradient operator, p – fluid pressure and η – fluid dynamic viscosity.

Solving the Reynolds-Averaged Navier-Stokes equations is not possible due to the lack of knowledge about the fluctuating variables contained in these equations. It is necessary to determine the Reynolds stresses $\overline{u'}\,\overline{u'}$ and turbulent diffusion to close the system of equations. To solve this problem, it is necessary to set up transport equations for the velocity correlation tensor and then model the third-order correlations. This model is known as the Reynolds Stress Model (RSM) and belongs to the class of Reynolds-Averaged Navier-Stokes (RANS) models.

Discrete phase

Within the software package Ansys Fluent [20], the pneumatic conveying of solid particles was modelled using the Discrete Phase Model (DPM). The discrete trajectories of solid particles are calculated using the Lagrangian approach. To apply the DPM method, it is necessary to define the velocity, position, temperature, and size of individual particles. The physical properties of the discrete phase and initial conditions are used to initiate the trajectory calculations. The actual calculations are based on analysing the forces acting on the particles, using local conditions in the continuous phase. Particle trajectories are computed based on the air velocity, following an estimation of local momentum balance [19, 20, 21].

$$\frac{d}{dt}x_p = u_p \tag{3}$$

$$\frac{d}{dt}u_p = \frac{18\eta_f}{\rho_p d_p^2}\frac{C_D Re_p}{24}\left(u_f - u_p\right) + f \tag{4}$$

where: u_p – represents velocity of the particle, d_p – diameter of the particle, x_p – position of the particle, ρ_p – density of particle material, u_f – fluid velocity, Re_p – the particle Reynolds number, C_D – the drag coefficient and η_f – the fluid's dynamic viscosity.

The first term $18\eta_f/\rho_p d_p^2$ stands for the drag force acting on a particle by surrounding fluid and the second term $C_D Re_p/24$ is a summary of all other forces that can act on a particle (the pressure gradient force, the buoyancy force, gravitational force, etc). In this paper, all other forces besides the Saffmann and the gravitational forces are omitted, the reason is due to the large value of the ratio between solid particles and gas. The term $u_f - u_p$ is factor for drag force. The previous

equation can also be presented in the form of the particle relaxation time:

$$\frac{d}{dt}u_p = \frac{1}{\tau_p}\left(u_f - u_p\right) + f \tag{5}$$

where: τ_p – the particle relaxation time calculated according to the following expression:

$$\tau_p = \frac{\tau_{p0}}{f(Re_p)} \tag{6}$$

where: τ_{p0} can be determined by:

$$\tau_{p0} = \frac{\rho_p\, d_p^2}{18\,\eta_p} \tag{7}$$

where: Re_p – represents the particle Reynolds number given by:

$$Re_p = \frac{\rho_f\, d_p |u_f - u_p|}{\eta_f} \tag{8}$$

where: ρ_f – fluid density.

Particle-wall rebound model

The collision between particles and a wall with a rough surface is depicted in Figure 1. In this case, it's assumed that the wall's surface roughness is uniform. In this modelling approach, at the moment of collision between a particle and the wall, the collision is assumed to be like a "blade" intersecting a plane, with its position determined by a coordinate system. The collision process is modelled based on the concept of a "virtual wall", as described in [22]. In order to take into account, the effect of wall roughness, a stochastic approach is adopted. A virtual angle is introduced to describe the wall's roughness.

Figure 2 shows the shadow effect is depicted, which is an additional effect of the "virtual angle" [23]. When a particle collides with the sheltered side of the rough wall surface, the velocity angle of the particle after the collision is negative (the particle is outside the computational domain).
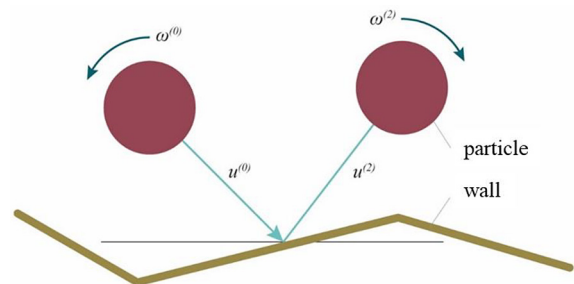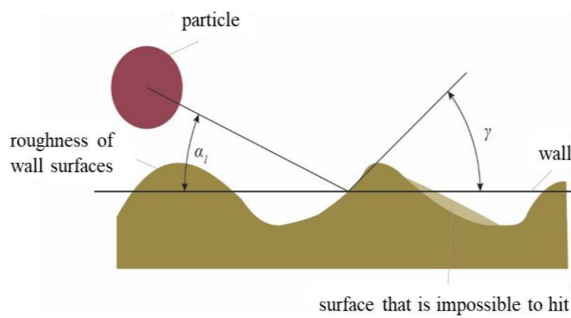

Fig. 1. Particle-wall collision

Fig. 2. Shadow effect

Furthermore, the probability of a particle impacting the front side of the rough wall surface is higher than the probability of it hitting the sheltered side (the shaded area in Figure 2). For this reason, the Gaussian distribution of the virtual angle function shifts towards positive values. The significance of shadow effects increases for smaller particles.

Finnie erosion model

The Finnie erosion model implies that the specific erosion rate on the surface, e (mass of eroded material / mass of particles impacting the material surface), can be expressed in the form of an equation [12, 24]:

$$e = K' |u|^n f(\alpha) \qquad (9)$$

where: α – the impact angle of the particle (the angle between the plane tangential to the surface at the point of impact and the direction of particle motion), u – particle velocity before impact, K' – scaling coefficient, n – the velocity exponent, which typically ranges from 2.3 to 2.7 for ductile materials and from 2 to 4 for brittle materials, $f(\alpha)$ – represents the dependence of erosion on the impact angle of the particle on the material surface and is defined as [12, 24, 25]:

$$f(\alpha) = \begin{cases} A_e\,\alpha^2 + B_e\alpha, \ \alpha \leq \varphi_k \\ X\cos^2\alpha\,\sin(W\alpha) + Y\sin^2\alpha + Z_e, \ \alpha > \varphi'_k \end{cases} \qquad (10)$$

where: A_e, B_e, W_e, X_e, Y_e, Z_e – empirical coefficients, φ_k – the impact angle of the particle on the material surface where maximum erosion occurs.

The coefficients utilized in Eq. 9 and 10 to predict solid particle erosion caused by sand particles on an aluminium plate and the impact angle of the particle on the material surface in the mathematical

Table 1. The erosion empirical coefficients and the impact angle of the particle [18, 26]

Coefficient	Value	Coefficient	Value
A_e	-7.0	X_e	0.4
B_e	5.45	Y_e	-0.9
K'	$1.7 \cdot 10^{-8}$	Z_e	1.556
n	2.3	W_e	-3.4
φ_k	23°		

model used for erosion calculation are extracted from [18, 26] and summarized in Table 1.

Modelling assumptions and numerical method

The fundamental input parameters for simulating erosion on an aluminum plate with a cylindrical hole caused by solid particles are provided in Table 2 [18]. Based on this information, it can be concluded that the mass ratio is very small, and the assumption made by the authors [18] that one-way interaction can be used is somewhat justified. However, in the current simulations, a two-way interaction has been implemented to increase the accuracy of the simulation. Among the thermophysical properties of aluminium, only density is considered in the model, with a value of $\rho_{Al} = 2700$ kg/m³, as presented in Table 2.

The erosion models investigated in this paper are based on experimental data from a study conducted by Wong et al. [18]. In their experiment, a test plate with a hole in the center is positioned perpendicular to the airflow and particles. Figure 3 provides a schematic representation of the

Table 2. The basic parameters for simulating erosion on the aluminum plate [18]

|	
Temperature	295 K
Fluid	Air
Fluid velocity	80 m/s
Fluid density	1.225 kg/m³
Fluid viscosity	$1.7894 \cdot 10^{-5}$ Pa s
The mean diameter of a sand particle	223 µm
Particle density	2650 kg/m³
Mass flow of sand	0.03 kg/s
Pipe material	Aluminium, ρ_{Al} = 2700 kg/m³
Turbulence model	RSM turbulence model
Differential scheme	QUICK
Model of particle collisions with the wall	Stochastic model
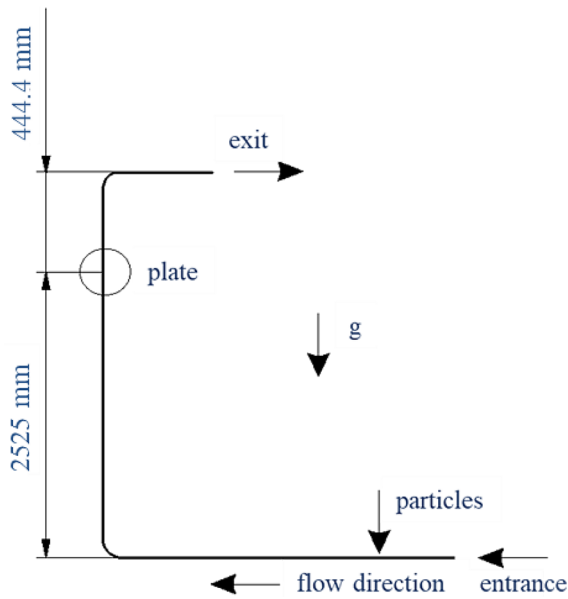
Fig. 3. Schematic representation of the experimental setup [18]

experimental setup [18], which includes the particle inlet point (pipe), a testing section, and an outlet section (pipe).

The test plate is made of aluminium, and the particles used are quartz sand. The aluminum plate dimensions are 84 mm (length) × 25 mm (width) × 2 mm (thickness), with a central cylindrical hole with a 7 mm diameter. The hole entrance is beveled at a 45° angle. The experimental setup and results are detailed in [18], from which a mathematical model was derived for calculating specific erosion metrics such as erosion rate, erosion depth, mean impact angle, particle velocity, and particle concentration on the cylindrical hole's surface within the aluminum plate.

The simulations were carried out using the Ansys Fluent software package [20], where the dispersed phase (quartz sand, with a particle mean diameter of $d_p = 223$ μm) is described by differential equations of motion, which are numerically tracked along trajectories with a constant particle number flow in a Lagrangian approach. The procedure for numerical modeling of two-phase flow with integrated submodels into Ansys software

involves a methodological process consists from: defining the problem by setting up the geometry and generating control volume meshes, boundary conditions, and initial settings, adjusting solver settings in Ansys to accommodate the specific requirements of integrated submodels, implementation of sub-models through User Defined Functions (UDF), numerical solving and analyzing the results (Figure 4). Afterward, a comparison was made between the simulation results and the experimental results of the paper [18].

The steps undertaken to improve the accuracy of our simulation results compared to the simulation conducted in the paper [18] are as follows:

- in the simulation conducted in this paper, both the vertical and horizontal parts of the pipe, as well as the elbow, are taken into account, unlike the simulation in [18] where only a part of the vertical pipe is simulated, and the initial position for calculating the trajectories is located 1m upstream of the plate (Figure 3). Since the length of the horizontal pipe is not provided in the paper [18], an assumed length of 2.5 m is used (Figure 5);
- a finer mesh was utilized in the immediate vicinity of the opening to enhance the accuracy of predictions in the CFD model in this paper. That resulted in a final mesh structure comprising approximately 1.2 million cells, while axial symmetry was used in the paper [18], simulating only one-quarter (a 90° segment) of the pipe;
- due to numerous collisions with the wall, the particles often change their direction of movement, and the angle at which they impact the aluminum plate is not always exactly 90°, and that was taken into account in this paper. Therefore, a stochastic model was employed in order to take into account the effect of wall roughness, while in the [18] it is assumed that the particles impact the plate at a high velocity at an angle of approximately 90°, without first having any collision with the wall;
- considering that the particle velocity is calculated according to the particle motion equation,
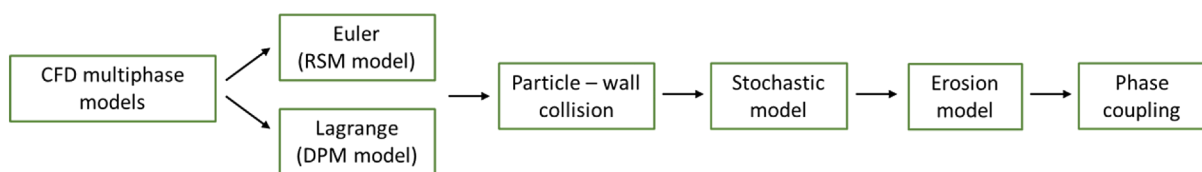

Fig. 4. Numerical model for two-phase flow

it can be assumed that the particle velocity is always less than the air velocity, especially after a long horizontal pipe and elbow, and given the numerous wall collisions that can be expected in this case. So, in this paper the particles start at the beginning of the horizontal pipe with an initial velocity of 0 m/s, while one of the assumptions in the paper [18] is that the initial velocity of the particles is equal to the mean air velocity and is 80 m/s.

In the first step, a 3D model of the two-phase flow of air and quartz sand particles was selected, and a structured hexahedral mesh was created, as shown in Figure 6. In the immediate vicinity of the opening, the cell side length is 0.1 mm, which was considered a sufficient size for accurate calculations. To create a mesh of this size for the entire geometry, tens of millions of cells would

be required, which, given the current computer capacity, would result in a very long simulation time. Therefore, the mesh was gradually coarsened as it moved away from the plate opening (towards the pipe walls or the pipe inlet). Numerical simulation results were obtained only from the part of the mesh in the immediate vicinity of the plate opening, and for this reason, this procedure is considered justified.

Initial and boundary conditions

The QUICK method was selected as the interpolation scheme, achieving the accuracy of a higher-order difference scheme as in the first case, while the flow near the wall is solved using the so-called "enhanced wall treatment". At the inlet of the pipe (Figure 5b), the air velocity is constant
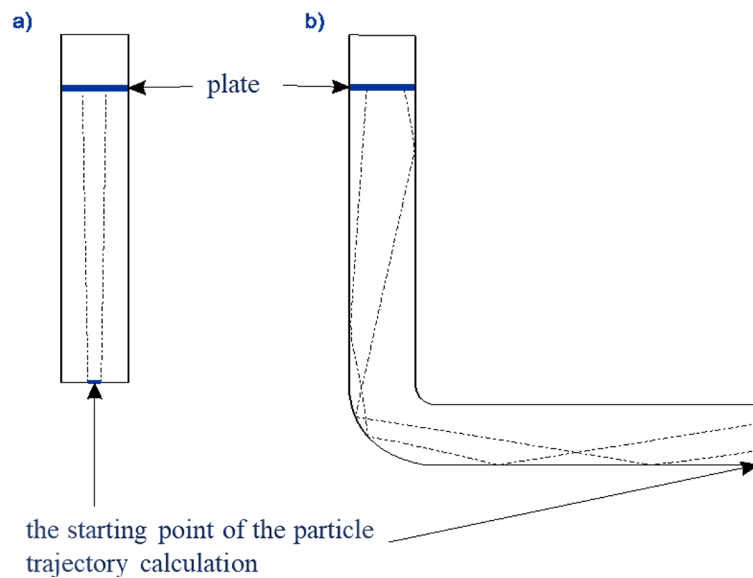

Fig. 5. Presentation of the plate's position and the initial point of particle trajectory calculation a) for the vertical part of the pipe, b) for the vertical and horizontal part of the pipe including elbow
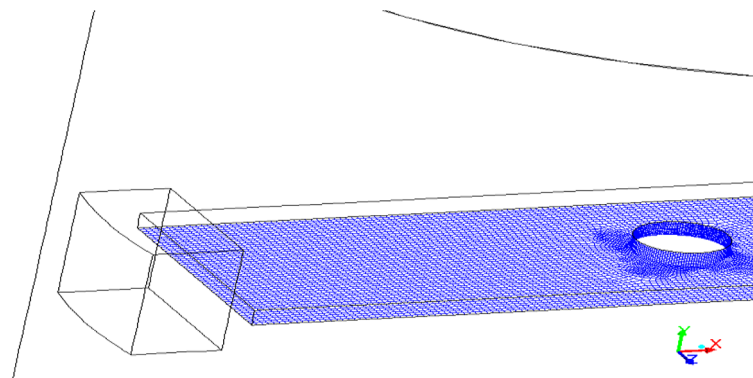

Fig. 6. Hexahedral mesh

and is 80 m/s. The outlet pressure is a boundary condition and is equal to the ambient pressure, which is 0 bar. First, the continuous phase is simulated, and after convergence, the calculation of the dispersed phase begins. The time step is equal to 10^{-3} s. The continuous and dispersed phases are calculated successively with 50 continuous phase iterations in one time interval and 1000 representative particle trajectories calculated in that time interval to achieve a stable solution with two-way interaction. Empirical coefficients used in the erosion calculation process, which are specific to a given particle/surface combination, for aluminium (the material of the test plate, the vertical part of the pipe, the horizontal part of the pipe, and the elbow) and quartz sand (particles) were taken from [18, 26] and are presented in Table 1.

RESULTS AND DISCUSSION

To calculate particle trajectories through the simulated geometry more accurately, additional sub-models were implemented. Sub-models include erosion and solid particle-wall collisions (stochastic model). Empirical coefficients are important for erosion calculation, while the stochastic model uses a virtual wall model. The normal coefficient of restitution for the combination of materials, quartz sand, and aluminum, as well as the static and dynamic coefficients of friction, remain the same as in the first case. Figure 7 shows particle trajectories, with the color of the particles indicating particle velocity in m/s.

In Figure 7, it can be seen that it takes some time after the elbow for the particles to homogenize again. The reason for this is the change in the direction of movement and frequent collisions

with the pipe wall. These are the reasons why the particle velocity is lower than the mean air velocity (80 m/s). On the left side of the image, it is also evident that many particles collide with the aluminum plate and then move downward (blue trajectories). These particles need to be accelerated again and have their direction changed. Therefore, multiple collisions with the plate are possible.

Particles after the elbow still have enough time to homogenize, resulting in the highest concentration in the middle of the plate (Figure 8). Since particles often change their direction of motion due to collisions with the wall, their angle of impact on the plate is not exactly 90°, so on average, particles are not moving purely vertically (Figure 9). The mean angle on the flat part of the plate is approximately 80°, and on the sloped part, it's around 60° (edges at the entrance to the cylindrical opening). The particle velocity varies across the surface of the plate. It is highest in the middle of the aluminum plate because the air
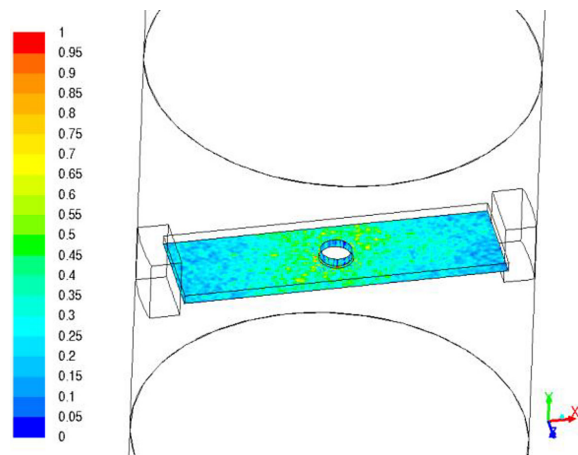

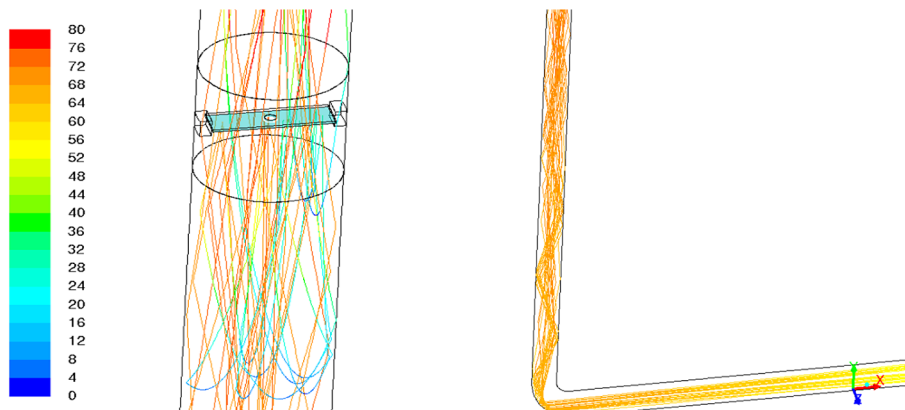**Figure 8.** Relative particle concentration (kg/m³) in the middle of the plate
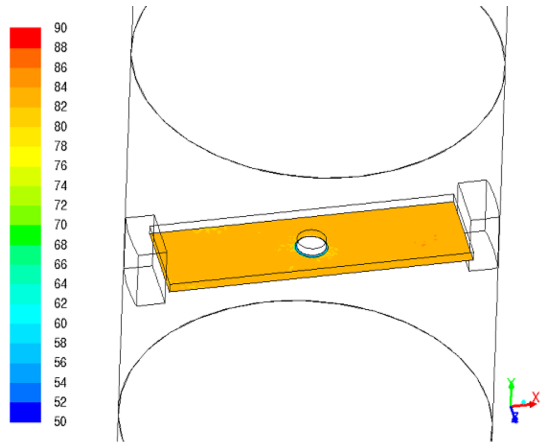

Fig. 7. Particles trajectories

Figure 9. Mean particle impact angle on the plate (°)
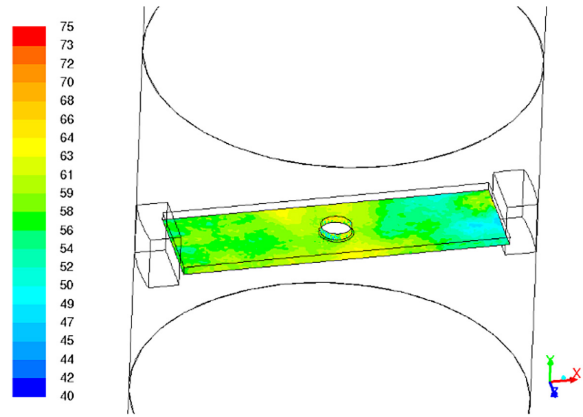

Fig. 10. Mean particle velocity magnitude of impact on the plate (m/s)
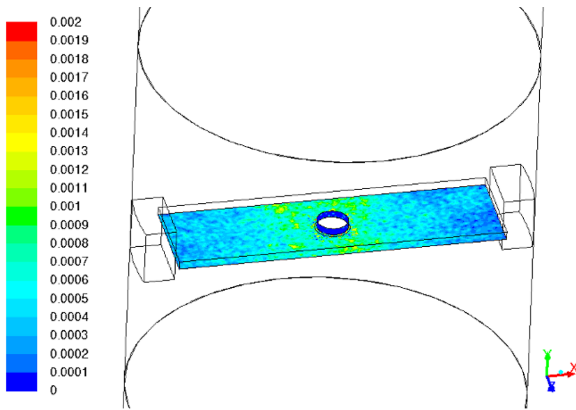

Fig. 11. Mean erosion rate (kg/(m²s))

velocity is highest in the middle of the pipe. Additionally, there is an opening in the middle where the air accelerates rapidly, causing the particles to accelerate at this point as well. The particle velocity decreases towards the edges of the plate, and one of the reasons could be the metallic components that support the plate (on the left and right in Figure 10). These components disrupt the flow, leading to a higher number of particle collisions with the plate in this area.

Due to the previously mentioned particle behavior (especially velocity), the erosion rate will not be uniform across the surface of the plate but
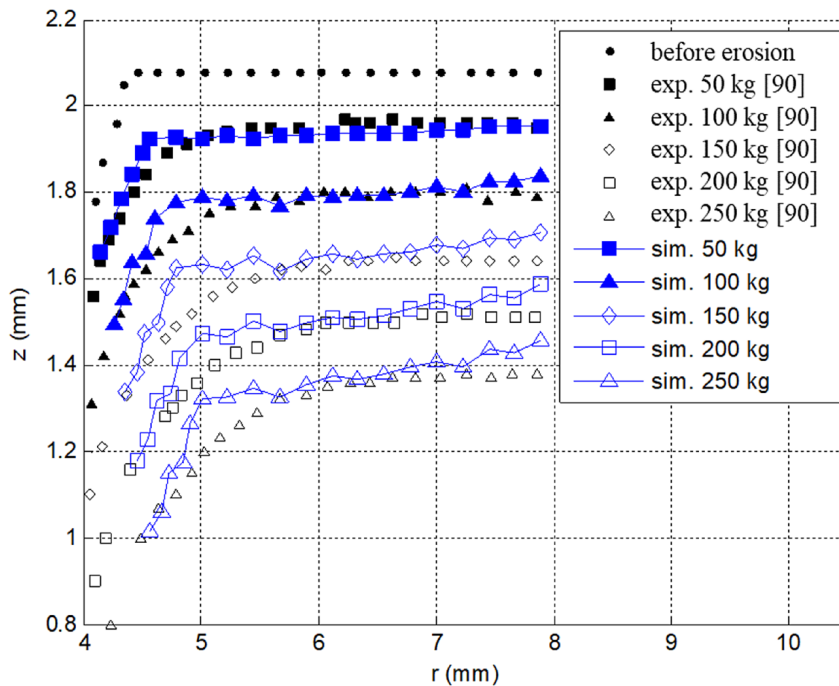

Fig. 12. Mean erosion depth (mm), or the surface profile of the plate after erosion, compared with the experimental results from the paper [18]

will be highest in the middle, gradually decreasing towards the edges of the plate. The surface profile of the plate after erosion is obtained by taking the mean erosion depth around the circumference of the hole at a certain radius. The surface profile of the plate after erosion is no longer perfectly horizontal because the erosion rate is not uniform across the plate's surface – it is highest in the middle and decreases towards the edges as can be seen from the Figure 11.

Figure 12 compares the numerical simulation results obtained in this paper with the experimental findings from [18]. It illustrates that the numerical results for the mean erosion depth (mm), representing the surface profile of the plate after erosion under loads of 50, 100, 150, 200, and 250 kg, obtained in this paper, more closely align with the experimental values compared to the simulation conducted in [18]. This improved alignment between simulation results and experimental values is attributed to enhancements made in the simulation model, as compared to the one used in [18].

It is necessary to note that the incubation effect was not considered during this simulation. The reason is that measurements began after the incubation time had already passed, so there are no experimental data for model verification. The incubation effect, or incubation time, refers to a period at the beginning of the erosion process during which the erosion rate is very small or negligible. It is only after this time that erosion increases, leading to the stabilization of the erosion rate. The exact reason for this material behavior is not fully understood. According to a common interpretation [12, 24], during this period, the material accumulates energy and undergoes plastic deformation. Cracking in the material and an increase in its hardness are possible. More intense damage is observed in the subsequent phase, leading to an increase in fluid turbulence in the immediate vicinity of the eroded surface.

CONCLUSIONS

In this paper, numerical simulations of erosion on an aluminum plate with a cylindrical hole caused by solid particles using the commercial software Ansys Fluent was performed. The study used RANS equations to predict fluid flow through an elbow, incorporating Euler-Lagrange particle tracking. To improve CFD accuracy, a finer mesh (about 1.2 million cells) near the

opening was employed. Additional sub-models were integrated for enhanced calculation of particle trajectories in the simulated geometry. These sub-models include collisions of solid particles with walls (stochastic model) and Finnie's erosion model. Using a virtual wall model within the stochastic approach improved accuracy, outperforming the standard deterministic model in Ansys Fluent. The conclusions drawn from the research are as follows:

- particles take time to homogenize after passing through the elbow, resulting in a velocity consistently lower than the mean air velocity;
- multiple wall collisions cause particles to deviate from a vertical path, with an average impact angle of about 80° on the flat plate and 60° on the beveled part;
- particle velocity varies on the aluminum plate, with the highest velocity in the middle due to accelerated air flow through the opening, and reduced velocity towards the plate's ends due to obstacles;
- erosion rates on the plate vary with particle velocity, being highest in the middle and gradually decreasing towards the edges;
- the numerical results in this paper better match experimental values than those in [18] due to enhancements in the simulation model.

Further work will be directed towards investigating the changes in wall roughness throughout the erosion process, as well as the analysis and comparison of the results with other erosion models.

REFERENCES

1. Sheng L.T., Xiao Y.L., Hsiau S.S., Chen C.P., Lin P.S., Jen K.K. A study of pneumatic conveying with high-density AM-using metal powder in a pipe bend. International Journal of Mechanical Sciences 2020; 181(1): 105763. https://doi.org/10.1016/j.ijmecsci.2020.105763

2. Herterich J.G., Griffiths I.M. A mathematical model of the erosion process in a channel bend. Tribology International 2021; 163: 107175. https://doi.org/10.1016/j.triboint.2021.107175

3. Hadžiahmetović H., Džaferović E., Ahmović I. The influence of parameters on the occurrence of erosion of system elements during pneumatic transport (in Bosnian). In: Proceedings of the 11th International Scientific Conference on Production Engineering, Sarajevo, Bosnia and Herzegovina 2017; 47–52.

4. Hashish M. An improved model of erosion by solid

particle impact. In: Proceedings 7th International Conference on Erosion by Liquid and Solid Impact, Cambridge, England 1987; 66: 1–9.

5. Hadziahmetovic H., Dzaferovic E. Ash pneumatic conveying from existing silos no. 4 to two new silos and ash loading in autocisterns. In: Proceedings of the 20th INTERNATIONAL DAAAM SYMPOSIUM "Intelligent Manufacturing & Automation: Theory, Practice & Education", Vienna, Austria 2009, 150–155.

6. Alghurabi A., Mohyaldinn M., Jufar S., Younis O., Abduljabbar A., Azuwan M. CFD numerical simulation of standalone sand screen erosion due to gas-sand flow. Journal of Natural Gas Science and Engineering 2021; 85: 103706. https://doi.org/10.1016/j.jngse.2020.103706

7. Zolfagharnasab M.H., Salimi M., Zolfagharnasab H., Alimoradi H. Shams M., Aghanajafi C. A novel numerical investigation of erosion wear over various 90- degree elbow duct sections. Powder Technology 2021; 380: 1–17. https://doi.org/10.1016/j.powtec.2020.11.059

8. Meng H.C., Ludema K.C. Wear models and predictive equations: Their form and content. Wear 1995; 181–183(2): 443–457. https://doi.org/10.1016/0043-1648(95)90158-2

9. Lain S., Sommerfeld M. Numerical prediction of particle erosion of pipe bends. Advanced Powder Technology 2019; 30(2): 366–383. https://doi.org/10.1016/j.apt.2018.11.014

10. Zhou J.W., Liu Y., Liu S.Y., Du C.L., Li J.P. Effects of particle shape and swirling intensity on elbow erosion in dilute-phase pneumatic conveying. Wear 2017; 380–381: 66–77. https://doi.org/10.1016/j.wear.2017.03.009

11. Nguyen V.B., Nguyen Q.B., Zhang Y.W., Lim C.Y.H., Khoo B.C. Effect of particle size on erosion characteristics. Wear 2016; 348: 126-137. https://doi.org/10.1016/j.wear.2015.12.003

12. Finnie I. Erosion of surfaces by solid particles. Wear 1960; 3: 87–103. https://doi.org/10.1016/0043-1648(60)90055-7

13. Li, B., Zeng, M., Wang, Q. Numerical simulation of erosion wear for continuous elbows in different directions. Energies 2022; 15(5): 1901. https://doi.org/10.3390/en15051901

14. Hong, B., Li, X., Li, Y., Li, Y., Yu, Y., Wang, Y., Ai, D. Numerical simulation of elbow erosion in shale gas fields under gas-solid two-phase flow. Energies 2021; 14(13): 3804. https://doi.org/10.3390/en14133804

15. Hadžiahmetović, H., Hodžić, N., Kahrimanović, D., Džaferović, E. Computational fluid dynamics (CFD) based erosion prediction model in elbows. Tehnički Vjesnik – *Technical Gazette 2014*; 21(2), 275–282.

16. Chen, X., McLaury, B.S., Shirazi, S.A. Application and experimental validation of a computational fluid dynamics (CFD)-based erosion prediction model in elbows and plugged tees. Computers & Fluids 2004; 33(10): 1251–1272. https://doi.org/10.1016/j.compfluid.2004.02.003

17. Pereira, G.C., de Souza, F.J., de Moro Martins, D.A. Numerical prediction of the erosion due to particles in elbows. Powder Technology, 2014; 261: 105–117. https://doi.org/10.1016/j.powtec.2014.04.033

18. Wong C.Y., Solnordal C., Swallow A., Wang S., Graham L., Wu, J. Predicting the material loss around a hole due to sand erosion. Wear 2012; 276–277: 1–15. https://doi.org/10.1016/j.wear.2011.11.005

19. Ferziger J.H., Peric M. Computational Methods for Fluid Dynamics, Springer, 2002.

20. Ansys Fluent 15.0 User Manual, ANSYS Inc., 2013.

21. Clift R., Grace J.R., Weber M.E. Bubbles, drops, and particles. Courier Dover Publications, 2005.

22. Sommerfeld M. Modelling of particle-wall collisions in confined gas-particle flows. International Journal of Multiphase Flow 1992; 18(6): 905–926. https://doi.org/10.1016/0301-9322(92)90067-Q

23. Sommerfeld M., Huber N. Experimental analysis and modelling of particle-wall collisions. International Journal of Multiphase Flow 1999; 25(6–7): 1457–1489. https://doi.org/10.1016/S0301-9322(99)00047-6

24. Finnie I. Some observations on the erosion of ductile materials. Wear 1972; 19: 81–90. https://doi.org/10.1016/0043-1648(72)90444-9

25. Finnie I., Kabil Y.H. On the formation of surface ripples during erosion. Wear 1965; 860–69. https://doi.org/10.1016/0043-1648(65)90251-6

26. Solnordal C.B., Wong C.Y. Predicting surface profile evolution caused by solid particle erosion. In Ninth International Conference on CFD in the Minerals and Process Industries, CSIRO, Melbourne, Australia 2012; 10-12.